Long-persistent luminescence from an exciplex-based organic light-emitting diode

Shinichi Tan, Kazuya Jinnai, Ryota Kabe, and Chihaya Adachi**

S. Tan, K. Jinnai, Prof. R. Kabe, Prof. C. Adachi
Center for Organic Photonics and Electronics Research (OPERA), Kyushu University
744 Motooka, Nishi-ku, Fukuoka 819-0395, Japan
E-mail: adachi@cstf.kyushu-u.ac.jp

S. Tan, K. Jinnai, Prof. R. Kabe, Prof. C. Adachi
JST, ERATO, Adachi Molecular Exciton Engineering Project
744 Motooka, Nishi-ku, Fukuoka 819-0395, Japan

Prof. R. Kabe
Organic Optoelectronics Unit, Okinawa Institute of Science and Technology Graduate University
1919-1 Tancha, Onna-son, Kunigami-gun Okinawa 904-0495, Japan
E-mail: ryota.kabe@oist.jp

Prof. C. Adachi
International Institute for Carbon Neutral Energy Research (I2CNER), Kyushu University
744 Motooka, Nishi-ku, Fukuoka 819-0395, Japan

Keywords: long-persistent luminescence, organic light-emitting diode, exciplex, charge separation, charge recombination

Abstract: Organic long-persistent luminescent systems (OLPLs) exhibiting long-lasting emission after photoexcitation are consisted of organic electron donors and acceptors, that are widely used in organic light-emitting diodes (OLEDs). Although OLPLs and OLEDs include very similar excitonic processes, long-lasting emission has never been observed in OLEDs. In this study, we confirmed the presence of long-persistent luminescence (LPL) under electrical excitation.

Glow-in-the-dark materials used in emergency lighting and watch indicators can store energy by photoexcitation and exhibit long-persistent luminescence (LPL) over several hours.[1–4] The present high-performance glow-in-the-dark materials are based on inorganic crystals, which require rare elements and high temperatures for fabrication.[5,6] In contrast, we recently reported glow-in-the-dark materials based on organic molecules that can be fabricated at room temperature through solution or melt-casting processes.[7,8] These organic long-persistent luminescence systems (OLPLs) are composed of a mixture of electron-donating and

electron-accepting materials, providing the unique functions of photoinduced charge separation, charge accumulation, and charge-recombination luminescence after photoabsorption.[9–11] Therefore, the emission process of OLPLs can be considered as a combination of that observed in organic solar cells (OSCs) and organic light-emitting diodes (OLEDs), because the photoinduced charge separation process between an electron donor and an acceptor[12–14] and the succeeding charge recombination luminescence process are fundamental in OSCs and OLEDs, respectively.[15,16] In particular, the intermolecular charge-transfer (CT) excited state between an electron donor and an acceptor, that is, the exciplex, plays an important role in the formation of the charge-separated state, which enables long-persistent energy storage and radiative decay (**Figure 1**(a)). Phosphorescence is also known as long-lasting photoluminescence, but the emission processes of phosphorescence and OLPL are completely different.[9,10] Phosphorescence is long-lived because the slow radiative transition rate from the triplet excited state to the singlet ground state, whereas OLPL is long-lived because the slow charge recombination[17].

The exciplex has attracted immense attention as a highly efficient OLED emitter owing to the inclusion of a thermally activated delayed fluorescence (TADF) process.[18–27] In particular, because the highest occupied molecular orbital (HOMO) tends to localize on a donor unit and the lowest unoccupied molecular orbital (LUMO) tends to localize on an acceptor unit in the exciplexes, the isolation of the HOMO and LUMO induces a small energy gap between the singlet and triplet excited states. Furthermore, because this small energy gap enables efficient thermal upconversion from triplet to singlet excited states, many exciplex systems exhibit TADF activity (Figure 1(b)).

A high external quantum efficiency (EQE) of more than 10% has been reported in OLEDs using 4,4',4-tris[phenyl(*m*-tolyl)amino]triphenylamine (*m*-MTDATA) as the donor and 2,8-bis(diphenylphosphoryl)dibenzo[b,d]thiophene (PPT) as the acceptor.[28] Moreover, this combination of *m*-MTDATA and PPT has also been reported as an efficient OLPL system.[8]

After the additional optimization of materials and device structures, EQE values of more than 20% were realized.[29] Moreover, high EQE values were reported by using exciplex as hosts for phosphorescence and TADF emitters.[30,31]

However, there have been no reports of LPL from exciplex OLEDs, and the correlation between OLEDs and OLPLs has not yet been clarified.[28] Considering the similarity of the emission mechanisms, we can expect LPL from OLEDs. Although it is rather difficult to find out the proper applications of LPL by OLEDs due to their weak brightness, LPL from OLEDs realizes unique long-term charge accumulation in organic semiconducting devices that may be applicable for future energy storage systems. Also, in contrast to the photo-induced charge separation of OLPL system, the LPL-OLEDs provide a unique exciton formation process starting from carrier injection, it would help us to understand the charge carrier dynamics of OLPL more specifically

In this study, we confirmed the presence of OLPL under electrical excitation. We have previously reported an afterglow OLED using a long-lived phosphorescent emitter, but this was a normal phosphorescent OLED, and the electroluminescence (EL) decay shows an exponential decay.[32,33] On the other hand, the afterglow OLED based on LPL shows a power-low EL decay (**Figure S1**). To obtain the observable LPL intensity after the current injection, a very thick emission layer (EML) and low donor concentration were required. To operate thick OLEDs, a high-voltage pulse was applied. We observed that the LPL emission intensity was dependent on the device thickness and on the pulse width of the applied voltage.

A combination of *m*-MTDATA and PPT, which has been used as an emitter in both OLPLs and exciplex OLEDs, was used in this study (Figure 1(c)). The major differences between OLPL and OLED are the donor-acceptor mixture ratio and the thickness of the emitting layer. Because OLEDs require high photoluminescence quantum yield (Φ_{PL}) and charge carrier balance, the typical donor concentration is approximately 30-70%,[28] whereas that in the case of OLPL is approximately 1%.[7] This is because the charge accumulation process is important

for OLPL, and the stored charges can be recombined immediately with neighboring donors when the donor concentration is high. For efficient charge injection, the film thickness required in conventional OLED EML is approximately 30 nm. Whereas, in the case of OLPL, because the number of stored charges depends on the film thickness, a thicker film of more than 1 μm is required to obtain an observable emission intensity.

First, to confirm the effect of the donor concentration, OLEDs with a 30 nm-thick EML with different donor concentrations were fabricated (**Figure S2**). It was observed that with decreasing donor concentration, the EL spectra were slightly blue-shifted; meanwhile the current density of *J-V* characteristics decreased because of the decreasing hole transport capabilities. However, an LPL component could not be detected from these OLEDs even at a donor concentration of 1%, which is the optimal concentration for the OLPL. This is because the film thickness is insufficient for realizing sufficient charge accumulation, which is crucial for achieving LPL.

The photophysical properties of the vacuum-codeposited films with thicknesses of 30 nm, 100 nm, and 300 nm indicate that the emission spectra were independent of the film thickness, but the emission duration and intensity increased with increasing film thickness (**Figure 2(a,b)**). This is because the number of accumulated charges depends on the film thickness. Further, various thicknesses of the OLED emission layer with a donor concentration of 1% were fabricated. Under electrical excitation, the typical film thickness (30 nm) of the OLED emitting layer exhibited a very faint LPL component after the electrical excitation was cut off, whereas the thicker films of 100 nm and 300 nm displayed appreciably higher LPL intensities (**Figure 2 (c,d)**). Moreover, the PL spectra were independent of the film thickness, whereas the EL spectra varied significantly. This spectral change can be attributed to the variation in the interference of light in the thick organic film and in the light outcoupling efficiency with different film thicknesses.[34] In addition, the EL spectra thus obtained are in good agreement with the simulated EL spectra obtained using semiconducting thin-film optics

simulation (Setfos) software (**Figure S3**). The emission peak at approximately 700 nm, which is only observed in the EL spectra, is expected to derived from the electromer of *m*-MTDATA in hole transport layer (HTL)[35–37]. Such emission peak at 700 nm was also observed in the 30 nm thick EML device with a low donor concentration. This is because the majority carriers in the EML are electrons, charge recombination also occurs at the interface between HTL and EML.

The thick OLEDs were operated using high-voltage pulses. The driving voltage drastically increased with increasing film thickness, as shown in Figure S4. When the OLED was driven by 10 ms-width 70 V pulses, the transient EL decay clearly exhibited a component that was delayed by more than 10 s (**Movie S1**). The emission decay profile is not that of an exponential decay, which can be observed for TADF or phosphorescence, but is that of a power-law decay similar to OLPLs (**Figure 2(d)**).[17] The LPL intensity was more than 1000 times weaker than the EL intensity during operation, we could not obtained the LPL emission spectra. The emission duration and decay profile indicates that the LPL emission originated from the EL of the exciplex. Therefore, the reason why no LPL could be observed in the previous *m*-MTDATA:PPT exciplex OLED is because of the thin fim and high donor-acceptor mixture ratio, which result in insufficient charge accumulation; therefore the presence of the LPL component could not be observed.

Further, because LPL was observed in thick-film OLEDs driven by high-voltage pulses, the dependence of the emission characteristics on the donor concentration, drive voltage, and pulse width were confirmed for the OLEDs with a 300-nm thick EML (**Figure 3 and Table S1**). The transient EL decay profiles of the OLEDs with donor concentrations of 5 mol%, 10 mol%, and 20 mol% indicate that the LPL duration decreases with increasing donor concentration (Figure S5). This trend is similar to that of the PL emission decay because the recombination probability of the accumulated charge carriers increases with increasing donor concentration. The effect of the pulse width and voltage was also investigated for OLEDs with

a donor concentration of 5 mol%. Longer LPL durations were observed for larger pulse voltages and longer pulse widths, thus providing a clear evidence of charge accumulation and successive LPL emission under electrical excitation.

Furthermore, to specify the charge recombination and accumulation position in the OLEDs, we fabricated reference devices without applying m-MTDATA doping to the emission layer (0 mol% of *m*-MTDATA). In addition, the hole transporting layer (HTL) of *m*-MTDATA was replaced by a 40 nm thick N,N'-di(1-naphthyl)-N,N'-diphenyl-(1,1'-biphenyl)-4,4'-diamine (α-NPD) and 10 nm thick 1,3-bis(N-carbazolyl)benzene (mCP) layers because the combination of mCP and PPT does not form an exciplex (Figure S6). As a result, the device without *m*-MTDATA (device D) exhibited no LPL. The LPL properties of the device without m-MTDATA doping (device B) were significantly reduced compared to that of device A. This indicates that only the interfacial exciplex between *m*-MTDATA and PPT contributed to the LPL. The device using mCP and α-NPD as the hole-transporting layer (device C) exhibited slightly lower performance than device A. These results suggest that charge accumulation occurs mainly within the EML, and that the contribution at the HTL/EML interface is small for carrier accumulation.

In conclusion, this study first confirmed the presence of LPL by photoexcitation as well as electrical excitation in exciplex OLEDs. In typical exciplex-based OLEDs, the LPL has not been reported so far because the charge recombination process is sufficiently fast owing to the good carrier balance and thin emission layer. The OLPL obtained by electrical excitation was clearly observed by reducing the donor concentration and increasing the film thickness to enhance the charge accumulation process. Further analysis of the charge accumulation and charge recombination processes of the exciplex-based OLEDs is required to gain improved understanding of the OLPL systems.

Experimental Section

Materials: PPT was prepared as described in the literature[38], while *m*-MTDATA was obtained from TCI Chemicals (Tokyo, Japan) and purified by sublimation.

Film fabrication: Glass substrates coated with a patterned indium tin oxide (ITO) layer with a thickness of 100 nm were used for OLED fabrication. ITO substrates were ultrasonically cleaned in the order of neutral detergent (Cica clean LX-II, Kanto Chemicals), two times of pure water, and two times of acetone for each 5 minutes, boiled in isopropanol at 270 degrees, and then under UV-ozone treatment for 15 minutes. Then, ITO substrates were transferred to a vacuum evaporation chamber. After the evacuation of the chamber to < 10^{-4} Pa, 35 nm thick *m*-MTDATA, emission layer, 35 nm thick PPT, 0.8 nm LiF and 100 nm thick Al layers were vacuum deposited on the ITO substrates to complete OLEDs. The active area of OLEDs was 2 mm × 2 mm. Neat films used for measuring the optical properties were fabricated on quartz substrates.

Optical and electrical Measurements: Absorption spectra were measured using a UV-vis-NIR spectrophotometer (LAMBDA 950, Perkin Elmer). Photoluminescence spectra were measured using spectrofluorometers (FluoroMax, Horiba Jobin Yvon; FP-8600, JASCO; and PMA-12, Hamamatsu Photonics). Absolute photoluminescence quantum yields (Φ_{PL}) were measured using an integrating sphere with a photoluminescence measurement unit (Quantaurus-QY, Hamamatsu Photonics).

LPL Measurements: LPL properties (spectra and decay profiles) were obtained using a measurement system in a glove box. Fabricated films were placed in the dark box and excited using a 340-nm LED (M340L4, Thorlabs) with a bandpass filter (340 ± 5 nm) at a fixed excitation power (100 μW cm^{-2}). PL and LPL spectra were recorded using a multichannel spectrometer (QE-Pro, Ocean Photonics). Emission decay profiles were obtained using a Silicon photomultiplier (C13366-1350GA, Hamamatsu Photonics) connected to a multimeter (34461A, Keysight). The LPL duration was defined as the time until the emission intensity dropped below 0.05 pW.

OLED analysis: The EL spectra and current density versus voltage, EQE versus current density of the OLEDs were measured by integrating sphere system (A10094, Hamamatsu Photonics). The transient EL decay profiles were obtained by a silicon photomultiplier (C13366-3050GA, Hamamatsu Photonics) connected to a multimeter (34461A, Keysight). The pulse voltage signal generated by the pulse generator (Sapphire Plus 9212+, Quantum Composers) was increased by the amplifier (HSA4101, NF Corporation) and applied to the OLEDs.

EL spectra simulation: The theoretical emission spectra were calculated by semiconducting emissive thin-film optics simulator (Setfos, Fluxim).[34] Thicknesses and refractive constants of each layer were shown in Figure S5. The spectrum of 1 mol% *m*-MTDATA doped PPT film was used as the emission spectrum. The distribution of exciplex in EML was given by the following formula, and the dipole orientation was set as isotropic.

$$Normalized\ exciplex\ density = e^{-\frac{x}{10}}$$ (x is defined in Figure S7)

Supporting Information
Supporting Information is available from the Wiley Online Library or from the author.

Acknowledgments
This work was supported by the Japan Science and Technology Agency (JST), ERATO, Adachi Molecular Exciton Engineering Project, under JST ERATO Grant Number JPMJER1305, Japan, the International Institute for Carbon Neutral Energy Research (WPI-I^{2}CNER) sponsored by the Ministry of Education, Culture, Sports, Science and Technology (MEXT), JSPS KAKENHI Grant Numbers JP18H02049, JP18H04522 and Core-to-core program. We thank M. Tanaka and N. Nishimura for helpful discussion and K. Kusuhara and N. Nakamura for their assistance with the preparation of PPT, NPD and mCP.

Received: ((will be filled in by the editorial staff))
Revised: ((will be filled in by the editorial staff))
Published online: ((will be filled in by the editorial staff))

References

[1] J. Xu, and S. Tanabe, *J. Lumin.* **2019**, *205*, 581.

[2] Y. Li, M. Gecevicius, and J. Qiu, *Chem. Soc. Rev.* **2016**, *45*, 2090.

[3] Z. Pan, Y.-Y. Lu, and F. Liu, *Nat. Mater.* **2012**, *11*, 58.

[4] P. Alam, N. L. C. Leung, J. Liu, T. S. Cheung, X. Zhang, Z. He, R. T. K. Kwok, J. W. Y. Lam, H. H. Y. Sung, I. D. Williams, C. C. S. Chan, K. S. Wong, Q. Peng, and B. Z. Tang, *Adv. Mater.* **2020**, *32*, 2001026.

[5] T. Matsuzawa, Y. Aoki, N. Takeuchi, and Y. Murayama, *J. Electrochem. Soc.* **1996**, *143*, 2670.

[6] K. Van den Eeckhout, P. F. Smet, and D. Poelman, *Materials.* **2010**, *3*, 2536.

[7] R. Kabe, and C. Adachi, *Nature* **2017**, *550*, 384.

[8] K. Jinnai, N. Nishimura, R. Kabe, and C. Adachi, *Chem. Lett.* **2019**, *48*, 270.

[9] N. Nishimura, Z. Lin, K. Jinnai, R. Kabe, and C. Adachi, *Adv. Funct. Mater.* **2020**, *30*, 2000795.

[10] Z. Lin, R. Kabe, K. Wang, and C. Adachi, *Nat. Commun.* **2020**, *11*, 191.

[11] K. Jinnai, R. Kabe, and C. Adachi, *Adv. Mater.* **2018**, *30*, 1870286.

[12] B. Kippelen, and J.-L. Brédas, *Energy Environ. Sci.* **2009**, *2*, 251.

[13] S. Shoaee, *J. Photonics Energy* **2012**, *2*, 021001.

[14] P. B. Deotare, W. Chang, E. Hontz, D. N. Congreve, L. Shi, P. D. Reusswig, B. Modtland, M. E. Bahlke, C. K. Lee, A. P. Willard, V. Bulović, T. Van Voorhis, and M. A. Baldo, *Nat. Mater.* **2015**, *14*, 1130.

[15] C. W. Tang, and S. A. VanSlyke, *Appl. Phys. Lett.* **1987**, *51*, 913.

[16] M. A. Baldo, S. Lamansky, P. E. Burrows, M. E. Thompson, and S. R. Forrest, *Appl. Phys. Lett.* **1999**, *75*, 4.

[17] P. Debye, and J. O. Edwards, *J. Chem. Phys.* **1952**, *20*, 236.

[18] M. Sarma, and K.-T. Wong, *ACS Appl. Mater. Interfaces* **2018**, *10*, 19279.

[19] Y.-S. Park, S. Lee, K.-H. Kim, S.-Y. Kim, J.-H. Lee, and J.-J. Kim, *Adv. Funct. Mater.* **2013**, *23*, 4914.

[20] H.-B. Kim, and J.-J. Kim, *J. Inf. Disp.* **2019**, *20*, 105.

[21] M. Chapran, E. Angioni, N. J. Findlay, B. Breig, V. Cherpak, P. Stakhira, T. Tuttle, D. Volyniuk, J. V. Grazulevicius, Y. A. Nastishin, O. D. Lavrentovich, and P. J. Skabara, *ACS Appl. Mater. Interfaces* **2017**, *9*, 4750.

[22] J. Zhao, C. Zheng, Y. Zhou, C. Li, J. Ye, X. Du, W. Li, Z. He, M. Zhang, H. Lin, S. Tao, and X. Zhang, *Mater. Horizons* **2019**, *6*, 1425.

[23] M. Colella, P. Pander, D. D. S. Pereira, and A. P. Monkman, *ACS Appl. Mater. Interfaces* **2018**, *10*, 40001.

[24] E. Angioni, M. Chapran, K. Ivaniuk, N. Kostiv, V. Cherpak, P. Stakhira, A. Lazauskas, S. Tamulevičius, D. Volyniuk, N. J. Findlay, T. Tuttle, J. V. Grazulevicius, and P. J. Skabara, *J. Mater. Chem. C* **2016**, *4*, 3851.

[25] Q. Wang, Q.-S. Tian, Y.-L. Zhang, X. Tang, and L.-S. Liao, *J. Mater. Chem. C* **2019**, *7*, 11329.

[26] T. Xu, J.-G. Zhou, C.-C. Huang, L. Zhang, M.-K. Fung, I. Murtaza, H. Meng, and L.-S. Liao, *ACS Appl. Mater. Interfaces* **2017**, *9*, 10955.

[27] B. Zhao, Y. Miao, Z. Wang, W. Chen, K. Wang, H. Wang, Y. Hao, B. Xu, and W. Li, *Org. Electron.* **2016**, *37*, 1.

[28] K. Goushi, and C. Adachi, *Appl. Phys. Lett.* **2012**, *101*, 023306.

[29] M. Chapran, P. Pander, M. Vasylieva, G. Wiosna-Salyga, J. Ulanski, F. B. Dias, and P. Data, *ACS Appl. Mater. Interfaces* **2019**, *11*, 13460.

[30] J. H. Lee, S. H. Cheng, S. J. Yoo, H. Shin, J. H. Chang, C. I. Wu, K. T. Wong, and J. J. Kim, *Adv. Funct. Mater.* **2015**, *25*, 361.

[31] Y. Danyliv, D. Volyniuk, O. Bezvikonnyi, I. Hladka, K. Ivaniuk, I. Helzhynskyy, P. Stakhira, A. Tomkeviciene, L. Skhirtladze, and J. V. Grazulevicius, *Dye. Pigment.* **2020**, *172*, 107833.

[32] R. Kabe, N. Notsuka, K. Yoshida, and C. Adachi, *Adv. Mater.* **2016**, *28*, 655.

[33] N. Notsuka, R. Kabe, K. Goushi, and C. Adachi, *Adv. Funct. Mater.* **2017**, *27*, 1703902.

[34] W. Youn, J. W. Lee, H. Yu, and D. Y. Kim, *ACS Appl. Electron. Mater.* **2020**, *2*, 2218.

[35] J. Kalinowski, G. Giro, M. Cocchi, V. Fattori, and P. Di Marco, *Appl. Phys. Lett.* **2000**, *76*, 2352.

[36] S. Kwon, K.-R. Wee, C. Pac, and S. O. Kang, *Org. Electron.* **2012**, *13*, 645.

[37] S. Wang, X. Wang, B. Yao, B. Zhang, J. Ding, Z. Xie, and L. Wang, *Sci. Rep.* **2015**, *5*, 12487.

[38] C. Fan, C. Duan, Y. Wei, D. Ding, H. Xu, and W. Huang, *Chem. Mater.* **2015**, *27*, 5131.

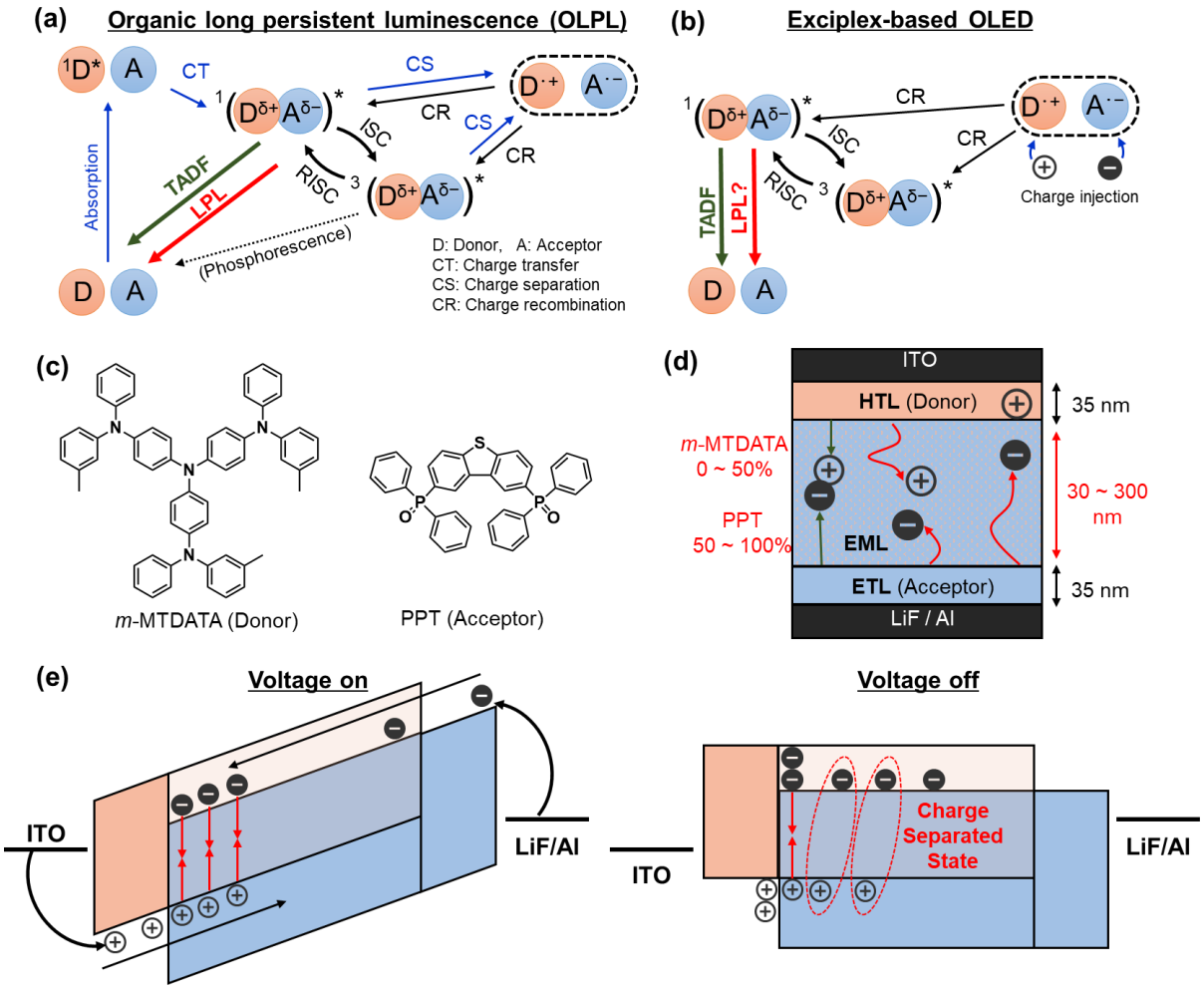

Figure 1. (a) Emission mechanism of OLPL. The singlet and triplet charge transfer (CT) excited states are formed by a fast CT process from the locally excited state of the donor or acceptor by photoexcitation. The subsequent charge separation (CS) process forms a stable radical ion pair. The recombination of the radical ion pairs leads to the formation of the CT excited states and exhibits LPL. Due to the presence of the reverse intersystem crossing (RISC) process, most of the emission originates from the singlet CT excited state. (b) Emission mechanism of exciplex-based OLED. The injected holes and electrons recombine and generate the singlet and triplet CT excited states. Due to the RISC process, most of the emission comes from the singlet CT excited state. (c) Chemical structures of the electron donor *m*-MTDATA and the electron acceptor PPT. (d) Device structure. HTL and ETL are consisted of *m*-MTDATA and PPT, respectively, and EML is consisted of *m*-MTDATA and PPT. (e) Schematic of carrier dynamics during and after applying voltage. Injected holes and electrons are recombined during pulse voltage is applied. After turn-off pulse voltage, the injected charge carriers accumulate in the EML and the EML-HTL interface and gradually recombine.

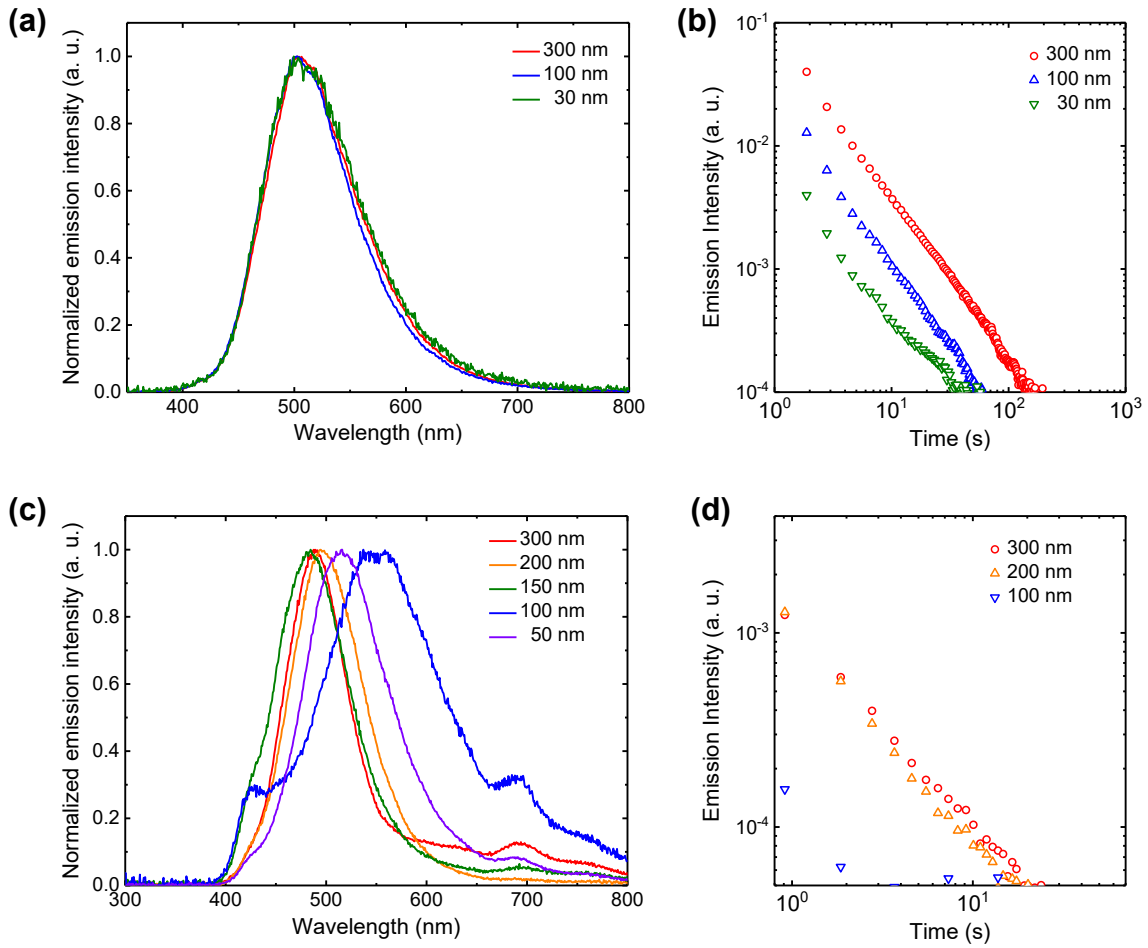

Figure 2. (a) Thickness dependence of the photoluminescence (PL) spectra of the co-deposited films with 1 mol% donor concentration. (b) PL transient decay profiles. (c) Thickness dependence of the EL spectra of the co-deposited films with 1 mol% donor concentration. (current density = 100 mA/cm^2) (d) EL transient decay profiles. (pulse voltage = 70 V and pulse width = 10 ms)

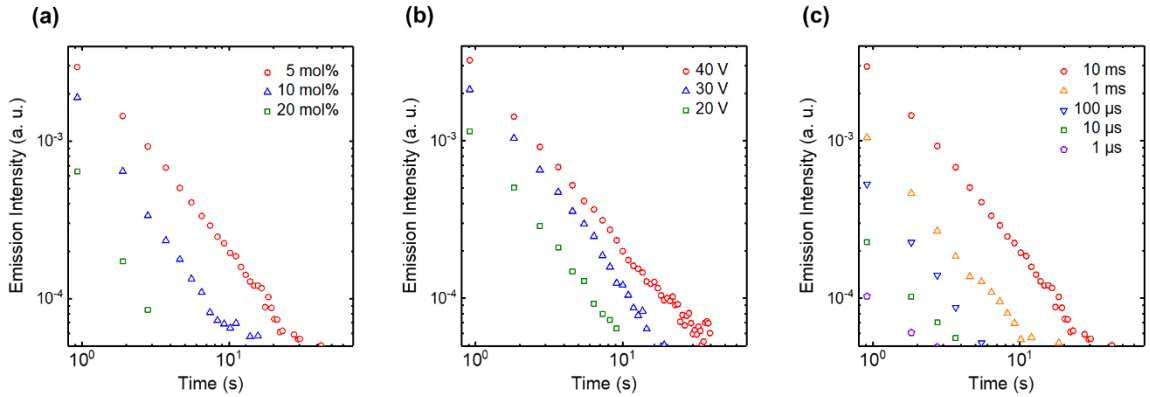

Figure 3. Dependence of the EL decay profiles on: (a) donor concentration (pulse voltage = 40 V and pulse width = 10 ms), (b) pulse voltage (donor concentration = 5 mol% and pulse width = 10 ms), and (c) pulse width (donor concentration = 5 mol% and pulse voltage = 40 V)

Keywords: long-persistent luminescence, organic light-emitting diodes, exciplex, charge separation, charge recombination,

Shinichi Tan, Kazuya Jinnai, Ryota Kabe, and Chihaya Adachi**

Long-persistent luminescence from exciplex-based organic light-emitting diode

ToC figure

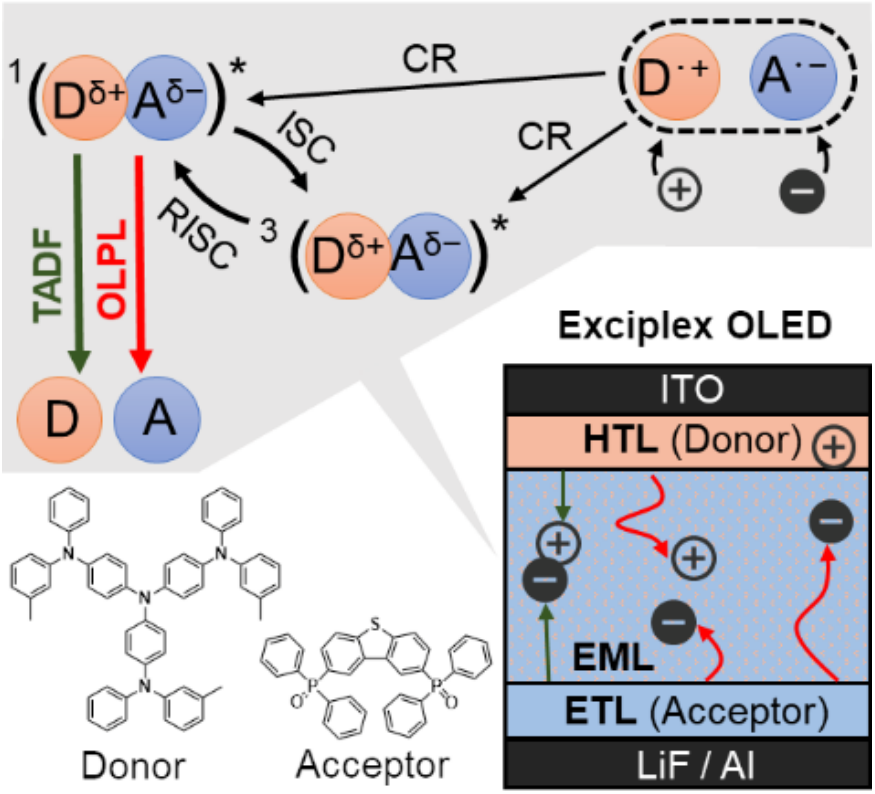

Supporting Information

Long-persistent luminescence from exciplex-based organic light-emitting diode

Shinichi Tan, Kazuya Jinnai, Ryota Kabe, and Chihaya Adachi**

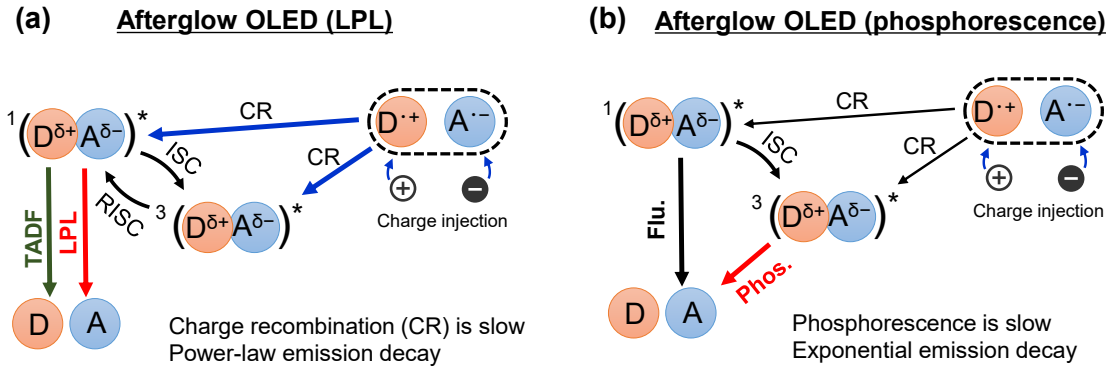

Figure S1. Emission mechanism of afterglow OLED based on LPL (a) and phosphorescence (b).

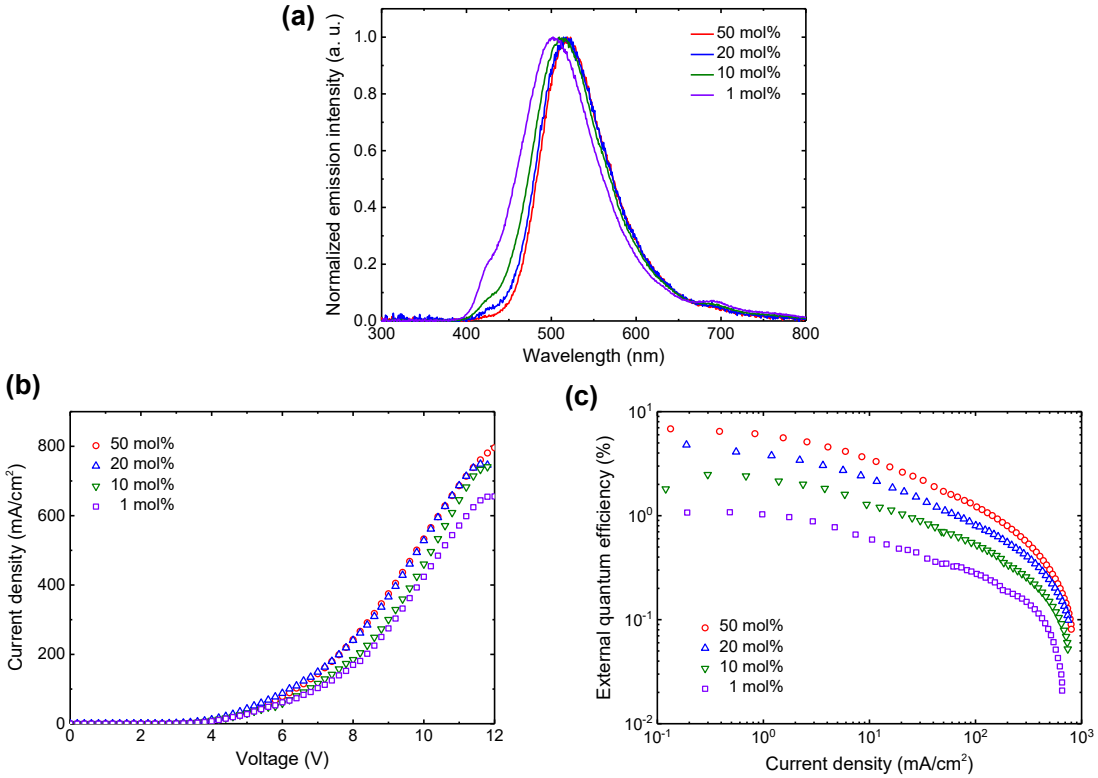

Figure S2. (a) EL spectra of the OLEDs having deferent concentration of *m*-MTDATA. (current density = 100 mA/cm^2) (b) *J*-*V* characteristics. (c) EQE vs. current density plots.

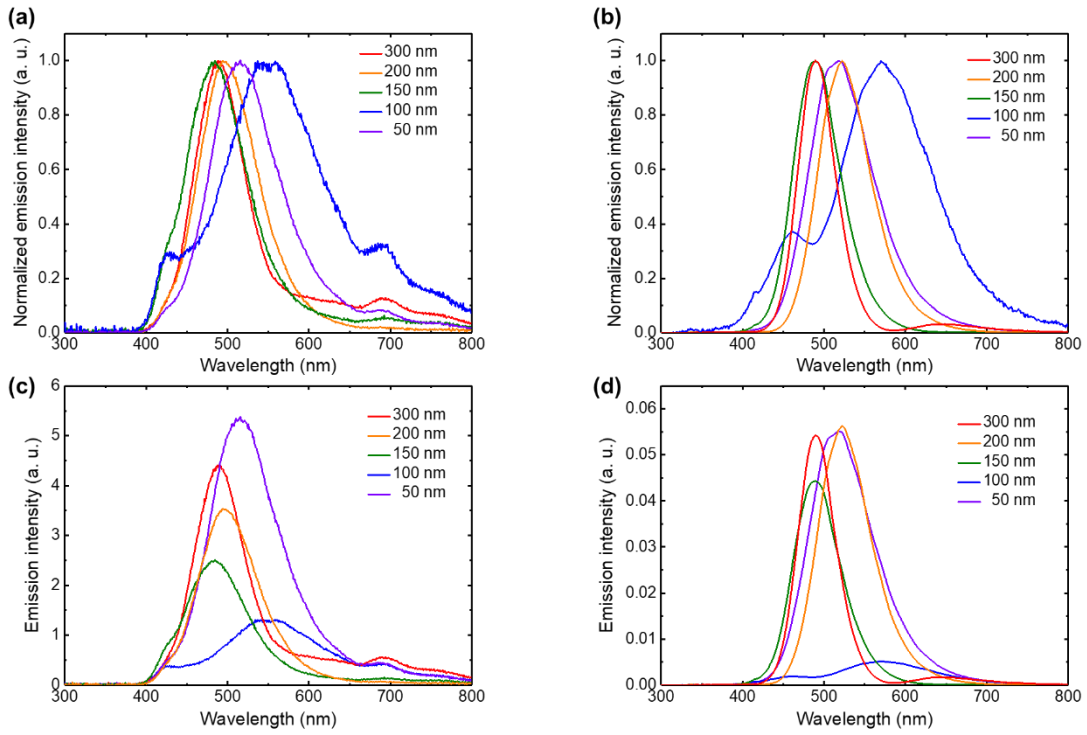

Figure S3. (a) Normalized EL spectra of OLEDs having a various thickness of the emission layer (Represent of Figure 2(c)). (b) Simulated normalized EL spectra of OLEDs having a various thickness of the emission layer. (c) Experimental non-normalized EL spectra of OLEDs having a various thickness of the emission layer. (current density = 50 mA/cm^2) (d) Simulated non-normalized EL spectra of OLEDs having a various thickness of the emission layer.

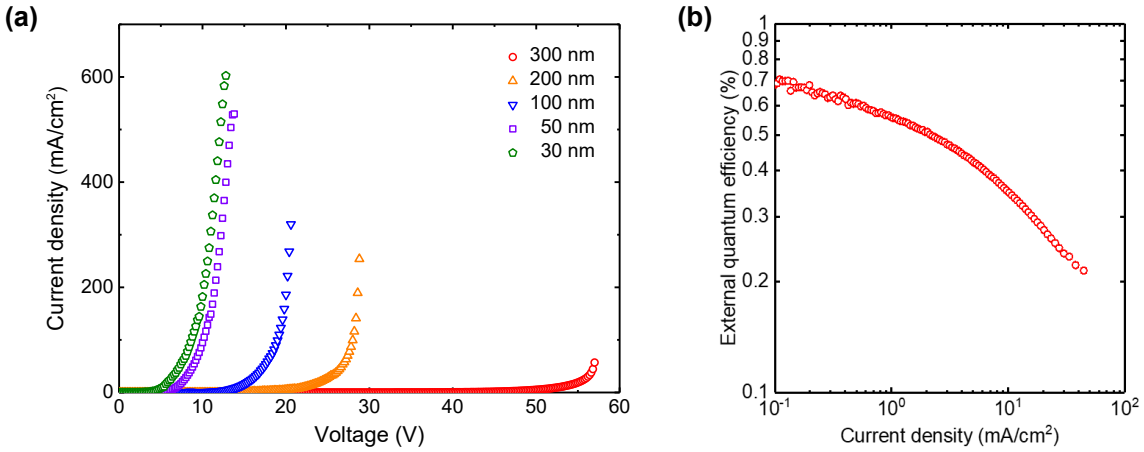

Figure S4. (a) *J-V* characteristics of OLEDs having a various thickness of the emission layer. (Donor concentration = 1 mol%) (b) EQE vs. current density plot of 300 nm EML device.

Table S1. OLED configurations and LPL characteristics

EML thickness [nm]	EML concentration [mol%]	Pulse voltage [V]	Pulse width [ms]	LPL duration[a] [s]
100	1	70	10	2
200	1	70	10	16
300	1	70	10	20
300	1	40	10	17
300	5	40	10	31
300	10	40	10	12
300	20	40	10	4
300	5	30	10	20
300	5	20	10	11
300	5	40	1	12
300	5	40	0.1	6
300	5	40	0.01	4
300	5	40	0.001	3

a: The LPL duration was defined as the time until the emission intensity dropped below 0.05 pW.

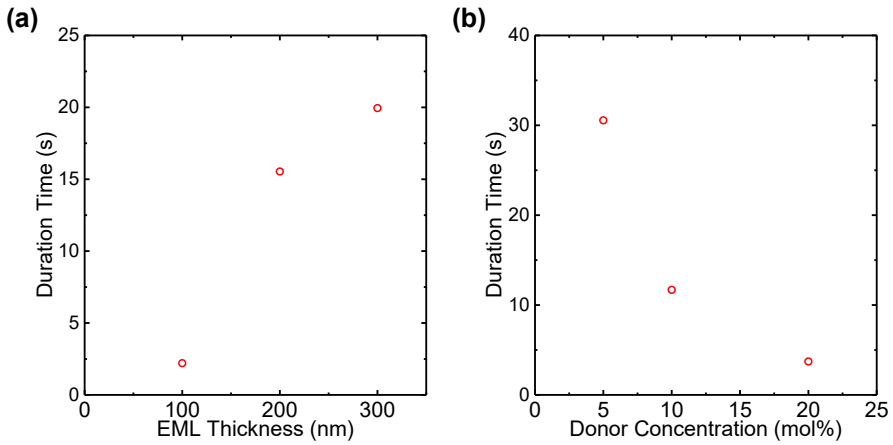

Figure S5. (a) Emission duration vs. EML film thickness. (b) Emission duration vs. donor concentration.

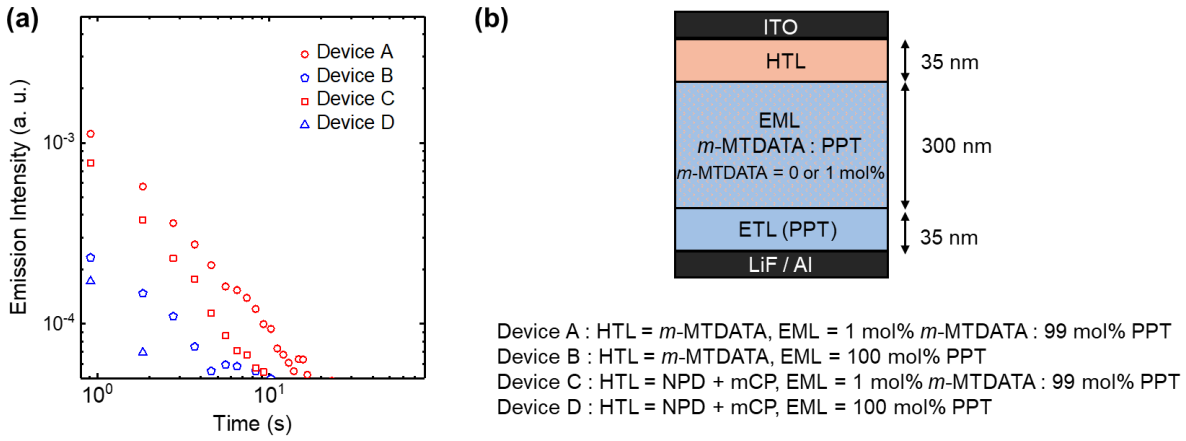

Figure S6. (a) EL emission decay profiles of OLEDs. (pulse voltage = 70 V and pulse width = 10 ms) (b) Device structure.

layer	Thickness	Refractive index
Glass	1 mm	Default value
ITO	100 nm	Default value
m-MTDATA	35 nm	1.7
EML	50 ~ 300 nm	Measured value of PPT
PPT	35 nm	Measured value of PPT
LiF	0.8 nm	Default value
Al	100 nm	Default value

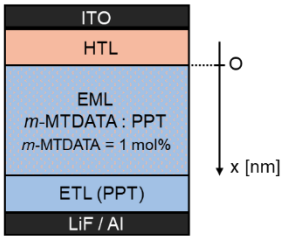

Figure S7. Parameters for simulation of EL spectra.